Journal of Crystal Growth 439 (2016) 33–39

Contents lists available at ScienceDirect

Journal of Crystal Growth

journal homepage: www.elsevier.com/locate/jcrysgro

X-ray diffraction study of GaSb grown by molecular beam epitaxy on silicon substrates

J.B. Rodriguez [a,b,*], K. Madiomanana [a,b], L. Cerutti [a,b], A. Castellano [a,b,c], E. Tournié [a,b,1]

[a] Université de Montpellier, IES, UMR 5214, F-34000 Montpellier, France
[b] CNRS, IES, UMR 5214, F-34000 Montpellier, France
[c] III–V Lab, Route de Nozay, F-91460 Marcoussis, France

ARTICLE INFO

Article history:
Received 16 November 2015
Received in revised form
5 January 2016
Accepted 9 January 2016
Communicated by H. Asahi
Available online 15 January 2016

Keywords:
A1. Heteroepitaxy
A1. X-ray diffraction
A2. Molecular beam epitaxy
B1. Antimonides
B1. Silicon substrate
B2. Semiconducting III–V materials

ABSTRACT

We report on the molecular beam epitaxy and characterization by X-ray diffraction techniques of GaSb layers grown on silicon substrates. AlSb and Al nucleation layers were used with different thicknesses and growth temperatures. Reciprocal space maps and a modified version of the Williamson-Hall analysis allowed for a characterization of the misfit dislocations properties. Finally, a post-growth annealing step is studied in order to further improve the material quality. Using this technique, a full-width-at-half-maximum of the GaSb peak of 235 arc sec was obtained for a layer thickness of 1 μm, which is comparable to the best results for GaAs or Ge on Si.

1. Introduction

Achieving hetero-epitaxy of III–V semiconductors on silicon substrate is of increasing interest as it would allow the realization of new photonics and microelectronics devices. Combining on the same chip the maturity of the CMOS technology to high-mobility and narrow band-gaps III–Vs, or the silicon photonics complex circuitry to III–V laser sources would indeed pave the way for a totally new generation of highly integrated devices. Although impressive results have been achieved using different types of bonding techniques, the epitaxy of the III–V material onto silicon remains the more attractive approach in terms of integration density and cost [1]. However, most of the III–V materials have a large lattice parameter mismatch with silicon; the thermal expansion coefficients are also significantly different and silicon is a non-polar material, which is of course not the case for III–Vs. For these reasons, III–V materials epitaxied on silicon generally exhibit a large density of defects such as threading dislocations, anti-phase boundaries (APD), micro-twins or cracks. In this context, the direct epitaxy of antimonide-based semiconductors appears promising and has already allowed demonstrating lasers operating in continuous-wave at room-temperature with a buffer thickness as low as 1 μm [2]. Although using these materials is not new, only a few papers have been published on the study and optimization of the nucleation steps and on the characterization of the grown material [3–7]. The general picture emerging from these studies is that an AlSb nucleation layer greatly improves the quality of GaSb buffers. The deposition of AlSb creates faceted islands at the surface of the silicon. These islands serves as nucleation sites for the subsequent growth of GaSb, and by decreasing the Ga diffusion length facilitates the transition towards a bi-dimensional GaSb layer [5,7]. The density and average size of the AlSb dots obviously depends on the growth conditions, and it is thus mandatory to exhaustively study their influence to maximize the beneficial effect on the GaSb layer quality. Micro-structure analysis also suggested that the strain relaxation process is mainly dominated by the formation of a well-organized array of edge dislocations located at the interface with the silicon substrate.

In this paper we report on X-ray diffraction analyses conducted on GaSb layers grown by molecular-beam-epitaxy on silicon substrates. Several growth conditions of the first steps of the epitaxy were explored, including various thicknesses and substrate temperatures of an AlSb nucleation layer. We also demonstrate that a good material quality can be achieved using a pure Al deposition before the GaSb growth. ω and $\omega-2\theta$ scans on a large variety of reflections together with reciprocal space maps of the GaSb layers were used to characterize the dislocation network. Finally, the

* Corresponding author at: Université de Montpellier, IES, UMR 5214, F-34000 Montpellier, France.
E-mail address: rodriguez@ies.univ-montp2.fr (J.B. Rodriguez).
[1] Member of Institut Universitaire de France (IUF).

http://dx.doi.org/10.1016/j.jcrysgro.2016.01.005
0022-0248/

post-growth annealing of the samples is explored and shows a significant improvement of the GaSb layer quality.

2. Experimental details

The samples have been grown by molecular beam epitaxy (MBE) in a reactor equipped with valved cracker cells providing element-five fluxes. Substrate temperature was monitored by standard pyrometry, while the different growth rates were calibrated by means of reflection high energy electron diffraction (RHEED) oscillations on GaSb substrates. Growth rates were set to 0.65 ML/s for GaSb and 0.35 ML/s for AlSb. The antimony flux was kept constant for both the AlSb and GaSb layers, resulting in V/III ratios of 1.5 and 3 respectively. Quarters of 2 in. (001) silicon substrates with a 6° offcut towards the [110] direction were used. The substrates were first prepared using cycles of HF dip and oxygen plasma exposure to obtain a flat and perfectly clean surface prior to loading in the MBE. The substrates were then flash annealed up to 800 °C inside the MBE, without impinging flux, to remove residual impurities of the surface. More detail on both the ex-situ and in-situ preparation of the silicon substrates can be found in Ref. [8]. At the beginning of the AlSb epitaxy, RHEED showed a spotty pattern, indicating a three-dimensional growth, changing to a (1×3) reconstructed pattern after 50–100 nm of GaSb was deposited, depending on the growth conditions. High-resolution X-ray diffraction (HR-XRD) measurements were carried out using a PANalytical X'Pert^3 MRD equipped with a PIXcel^{1D} linear detector, a four bounce asymmetric Ge(220) monochromator and an X-ray tube providing Cu $K_{\alpha 1}$ radiation. The ω and $\omega-2\theta$ scans were recorded with the PIXcell^{1D} in the open detector configuration which corresponds to a 2.5° aperture angle. A monochromator was added on the diffracted beam path for the triple-axis analysis. Reciprocal space maps were obtained with the same setup as for rocking curves in a grazing exit diffraction geometry on the $(\bar{2}\,\bar{2}\,4)$ peaks.

3. Results and discussion

3.1. Influence of the nucleation layer growth temperature and thickness on GaSb X-ray diffraction properties

The samples studied in this section comprise an AlSb nucleation layer, followed by a 50 nm thick layer of GaSb grown at the same temperature than the AlSb. The growth is then interrupted, and the substrate temperature is changed to 450 °C under Sb flux. A 450 nm thick GaSb layer is then deposited. Using this procedure, most of the GaSb buffer layer is grown in the same conditions for all the samples, allowing a fair comparison of the X-ray diffraction peak properties. The nucleation layer is encapsulated by the first 50 nm of GaSb before the substrate temperature change in order to limit any evolution of its morphology during this step. Finally, a quantum-well (QW) structure based on GaInAsSb QWs embedded in AlGaAsSb barriers is also grown. Photoluminescence data confirm the XRD trend. However, a detailed PL analysis is beyond the scope of this paper. Three sets of samples with the nucleation layer grown at 400, 450 and 500 °C have been studied. For each temperature, several samples with AlSb nucleation layer thicknesses from 0 to 150 monolayers (MLs) were grown. From XRD ω-scans (double crystal rocking curves with open detector), full-width-at-half-maximum (FWHM) of the (004) GaSb peaks were extracted and compared. The results are summarized in Fig. 1 showing the variation of the FWHM with the AlSb thickness for the three growth temperatures. A large variation of the FWHM can be observed confirming the importance of the growth conditions

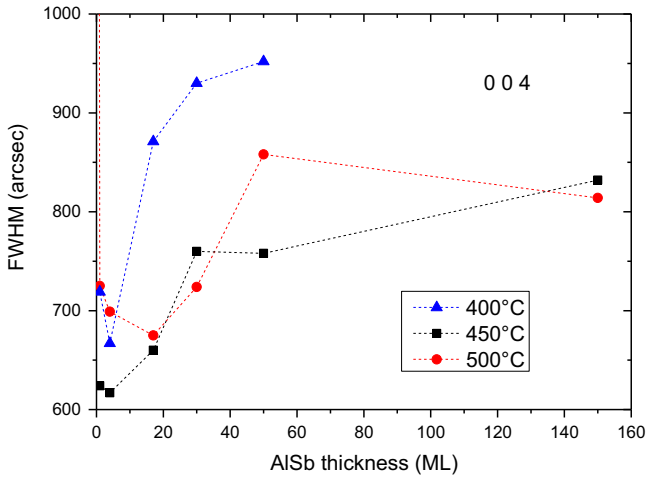

Fig. 1. Variation of the FWHM of the 004 GaSb peaks with the AlSb nominal thickness for different substrate temperature during the nucleation layer growth.

during the very first step of the nucleation on the material quality. First of all, the crucial role of AlSb is evident. For comparison sake, a GaSb layer was grown at 450 °C without any AlSb nucleation layer. The FWHM obtained for this sample was nearly 4200 arc sec whereas the samples with AlSb all resulted in FWHMs well below 1000 arc sec (the value for 0 ML is not shown in Fig. 1 for clarity sake), whatever the AlSb thickness. It is noticeable that the deposition of an AlSb nucleation layer as thin as 1 ML of AlSb before the GaSb buffer growth has already a drastic effect on the material quality, which is in agreement with previous reports.

The optimal AlSb thickness remains close for the three sets of samples and seems to slowly evolve from ~1–4 MLs at 400 °C to ~17 MLs at 500 °C. This latter value was also found to be the one giving the best material in reference [6], but the influence of the temperature on the optimal value was not explored, and it appears from our data that a substrate temperature of 450 °C is more favorable for the nucleation layer growth. For the three substrate temperatures explored in this study it is remarkable that the obtained data curves can all be decomposed in three different regions: the material quality first improves very rapidly, and then degrades very rapidly before becoming almost independent on the AlSb thickness. This is especially clear for the plot at 500 °C, and the different regions have been delimited in Fig. 2a. One possible explanation for this observation is that the GaSb layer quality strongly depends on both the AlSb dots density sitting on the silicon surface and on the number of coalescence of these dots. We describe in Fig. 2b what could be the main characteristics of the AlSb nucleation layer for each region. In the first region (e.g. when the nominal AlSb layer thickness is small), any additional AlSb deposited mainly results in an increase of the AlSb dot density. The number of nucleation sites for the GaSb growth also increases which improves the material quality. In this region, the number and size of AlSb dots increases, but the coalescence of dots is still a marginal process. By contrast, when the AlSb dot density has reached its maximum, increasing the AlSb nominal thickness will favor the coalescence of the dots. In this scenario, the optimum AlSb thickness thus corresponds to the situation where the maximum AlSb dot density has been reached, and the main process occurring in the second region (R2 in Fig. 2) is the coalescence of the AlSb dots. Once all the dots have coalesced, a two-dimensional layer of AlSb is formed and no more coalescence can occur (R3). The material quality in this region becomes dependent on other parameters such as the roughness or uniformity of the 2D AlSb layer for instance. The steep degradation of the FWHM in R2 implies that the defects created during the coalescence of the AlSb

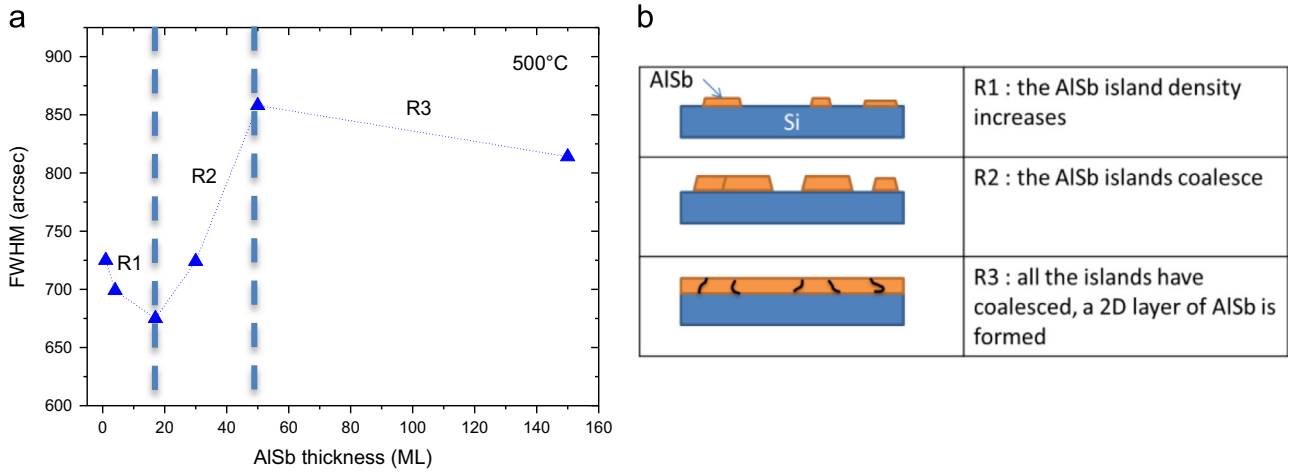

Fig. 2. Decomposition of the variation of the FWHM with AlSb nominal thickness at 500 °C in three regions (a), and possible AlSb configuration in the three regions (b).

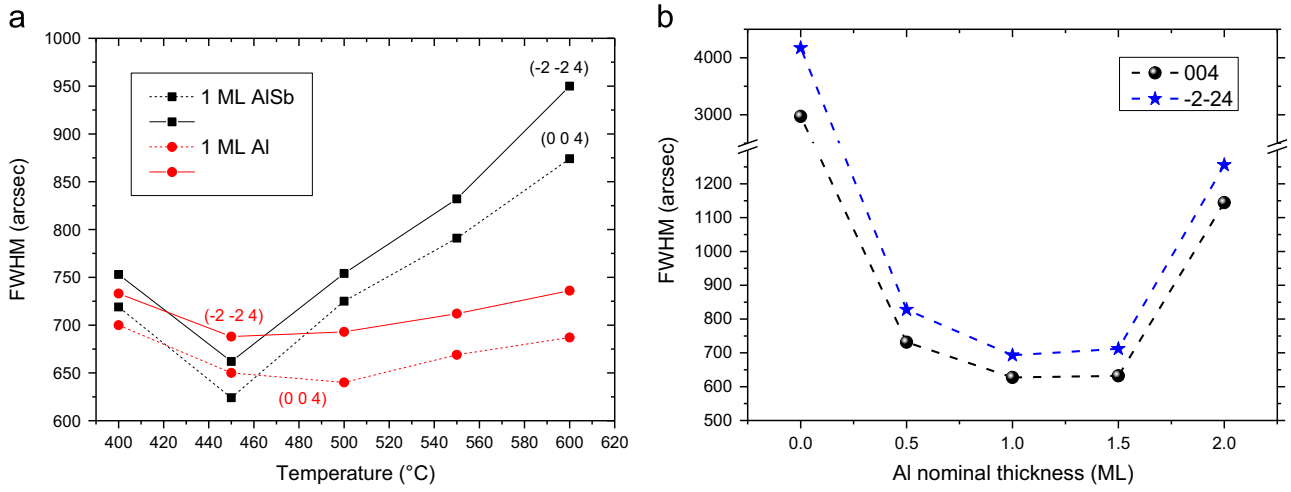

Fig. 3. Comparison of the FWHM of the GaSb peak when 1 ML of AlSb or pure Al is deposited prior to the GaSb growth (a); variation of the FWHM with the Al nominal thickness.

dots have a very negative impact on the quality of the upper layers, and must be avoided. In R1 and for a given nominal AlSb thickness, decreasing the substrate temperature results in an increase of the dot density and a decrease of the dots height. The maximum dot density is therefore reached for smaller nominal thicknesses of AlSb, and the optimal value is also smaller as the substrate temperature is decreased, which is coherent with our observation. The degradation observed for thicknesses above the optimal value is also steeper as the substrate temperature is decreased, which can be ascribed to the fact that the coalescence of the dots happens at a much faster rate at low temperature. In fact, at 400 °C the coalescence starts after a few MLs are deposited, and the 2D layer is completed within the first 20 MLs. By contrast, 5 nm of AlSb are needed at 500 °C for the dots to start coalescing and 15 nm before all the dots have coalesced due to the larger diffusion length of the atoms on the silicon surface.

3.2. *Replacing AlSb by a pre-deposition of pure Al*

AlSb has been traditionally used as a nucleation layer for the growth of GaSb on silicon. It was described in previous paragraphs that even a very small amount of AlSb is sufficient to drastically improve the GaSb quality. AlSb and GaSb have a common atom, antimony, and we can easily come to the natural conclusion that the beneficial effect of the AlSb has certainly to do with the presence of the Al atoms. In order to verify this statement, we have decided to explore the possibility to use a pure Al deposition before the growth of GaSb instead of the standard AlSb nucleation layer. Two sets of samples were grown comprising in both cases a 500 nm thick GaSb buffer layer (with again the first 50 nm grown at the same temperature than the nucleation layer and the upper 450 nm grown at 450 °C) and a QW stack grown at 450 °C. The only difference between the two sets was the nucleation layer composition, 1 ML of AlSb in one case and 1 ML of Al in the other. The nucleation layer was grown at various substrate temperatures in the 400–600 °C range. ω-Scans (double crystal rocking curves with open detector) were then recorded for the 004 and $\overline{2}24$ reflections and the FWHM of the GaSb peak calculated. The result is shown in Fig. 3a displaying the FWHM versus the temperature for the AlSb and the Al nucleation layer. In the case of the AlSb nucleation layer, the data shows a clear optimum temperature close to 450 °C, with a FWHM on the 004 reflection of 625 arc sec. The most interesting feature that can be highlighted from this graph is the fact that Al alone is as efficient as AlSb as a nucleation layer. Indeed, the best result of the Al set is obtained at 500 °C, with a FWHM of 634 arc sec, within 10 arcsec of the best value of the AlSb set of samples. On the other hand, results at 450 and 500 °C are very close to each other in terms of FWHM for the Al

set, which is not the case for AlSb where a clear degradation of about 100 arcsec is observed. This makes the optimal growth parameters window for the Al nucleation layer far wider, which is particularly interesting from a practical point of view: the possible variations due to the V/III ratio are not relevant in this case, and there is a relative insensitivity to the substrate temperature in a range larger than 50 °C. The only remaining parameter is the nucleation layer thickness. An additional set of samples with nominal Al thicknesses of 0.5, 1, 1.5 and 2 MLs deposited at 500 °C was realized to get a better insight on the thickness dependence on the material quality. The variation of the FWHM in 004 and $\bar{2}\bar{2}4$ with the thickness is shown in Fig. 3b (*double crystal rocking curves with open detector*). Again, an impressive improvement is obtained with the deposition of only 0.5 ML of Al, with FWHM decreasing very rapidly from 4000 arcsec down to below 1000 arcsec. The best FWHM is obtained for 1 ML, but values measured for 1.5 ML are very close, with an optimal value probably in between those two values. The growth parameters window appears again sufficiently large for practical use, despite the absence of an element V during the nucleation layer growth.

In summary, both the AlSb and the pre-deposited pure Al layers significantly improve the GaSb material quality. The use of AlSb requires a more careful adjustment of the substrate temperature than Al, whose deposited nominal thickness has to be in the 0.5–1.5 ML range. By comparing the FWHM of the X-ray diffraction peaks of several samples grown with various AlSb thicknesses, we have identified three different regions and proposed a scenario that enables describing the AlSb layer configuration during the growth, and its effect on the GaSb layer quality. However, at this point, no information on the origin of the broadening of the X-ray peaks can be deduced based on the previous analysis. In Section 3.3, we show that this broadening can give us a better insight on the misfit dislocation properties.

3.3. Misfit dislocation properties

For analyzing the properties of the misfit dislocations by X-ray diffraction, we carried out a more in-depth study on a sample using the best configuration obtained previously at 500 °C with the AlSb nucleation layer. It thus comprises a 5 nm thick AlSb nucleation layer grown at 500 °C, and a 1 μm thick GaSb buffer was used. The $\omega-2\theta$ scan (*double crystal measurement with open detector*) of the 004 reflection is shown in Fig. 4. Both the GaSb and the Si peak are clearly visible on the experimental curve. The

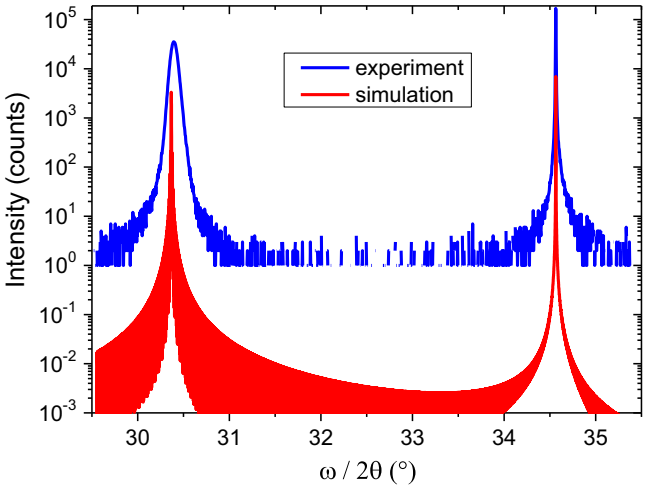

Fig. 4. Experimental (blue) and simulated (red) 004 $\omega-2\theta$ scan.(For interpretation of the references to color in this figure legend, the reader is referred to t-the web version of this article.)

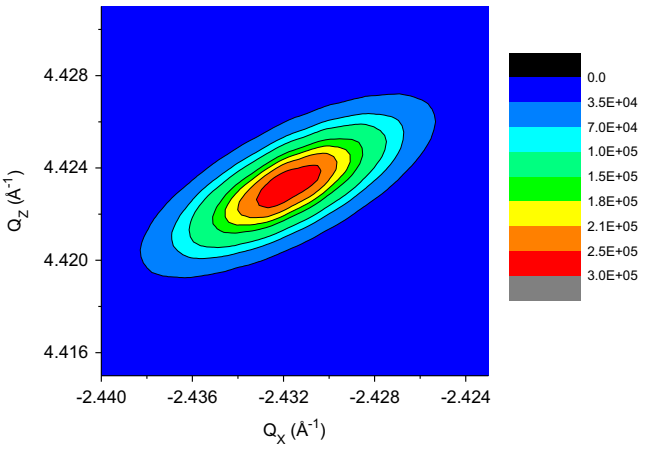

Fig. 5. Reciprocal space map of the $\bar{2}\bar{2}4$ GaSb peak.

simulated curve for a fully relaxed layer of GaSb is also shown in red. The mismatch between simulated and experimental GaSb peak position corresponds to a residual tensile in-plane strain of about 0.1%, ascribed to the difference of thermal contraction of GaSb and Si, when the sample is cooled down from growth to room temperature.

The reciprocal space map of the $\bar{2}\bar{2}4$ reflection of the GaSb peak is shown in Fig. 5. In this figure, Q_x and Q_z are the reciprocal lattice coordinates of the reciprocal lattice vector Q. They can be expressed in terms of ω and 2θ using $Q_x=\frac{2\pi}{\lambda}[\cos(\omega)-\cos(2\theta-\omega)]$ and $Q_z=\frac{2\pi}{\lambda}[\sin(\omega)+\sin(2\theta-\omega)]$, where λ is the wavelength of the copper $k_{\alpha 1}$ line used by the diffractometer. As expected from such a mismatched heteroepitaxial layer [9], the diffraction peak has an elliptical shape, and the FWHM in the in-plane (Q_x) and growth (Q_z) directions can be extracted. The ratio of these FWHM values ($\Delta Q_z/\Delta Q_x$) was suggested to be characteristic of the type of dislocations existing at the interface [9]. In this particular case, we found $\Delta Q_z/\Delta Q_x \sim 0.6$, which, according to the theory, is the signature of the predominance of 90° dislocations at the interface (60° dislocations would result in a ratio close to 0.3).

A more detailed analysis of the misfit dislocation network at the interface can be obtained using a modified version of the so-called Williamson-Hall plot [10]. In this analysis, the diffraction peak broadening (Δq) is related to the intrinsic properties of the misfit dislocation network, namely the spacing between the dislocations and the uniformity of this value, and finally the type of dislocations populating this network. This relationship can be written as

$$\Delta q = K\sqrt{\frac{\gamma\rho}{d,}} \qquad (1)$$

where d is the layer thickness, ρ is the dislocation density and γ is a correlation factor corresponding to the mean variation of the spacing between the dislocations. K is a coefficient which depends on the reflection orientation, the type of dislocation and the type of set-up configuration used (triple or double axis). The coefficient K can be calculated for 60° and edge dislocations for any orientation, or found in the literature [10,11]. In the present study, the 002, 004, 006, 115, $\bar{1}\,\bar{1}5$, 117, $\bar{1}\,\bar{1}7$, $\bar{2}\,\bar{2}4$, 335 and $\bar{3}\,\bar{3}5$ reflections were measured in both the double and triple axis geometry of the diffractometer. The FWHM of the GaSb peaks were extracted from the ω and $\omega-2\theta$ scans, and the value expressed in reciprocal space units. Finally, the broadening was plotted against the value of K corresponding to the measurement orientation. Fig. 6a shows the result when the K values for 60° dislocations are used, whereas the K values for edge dislocations are considered in Fig. 6b.

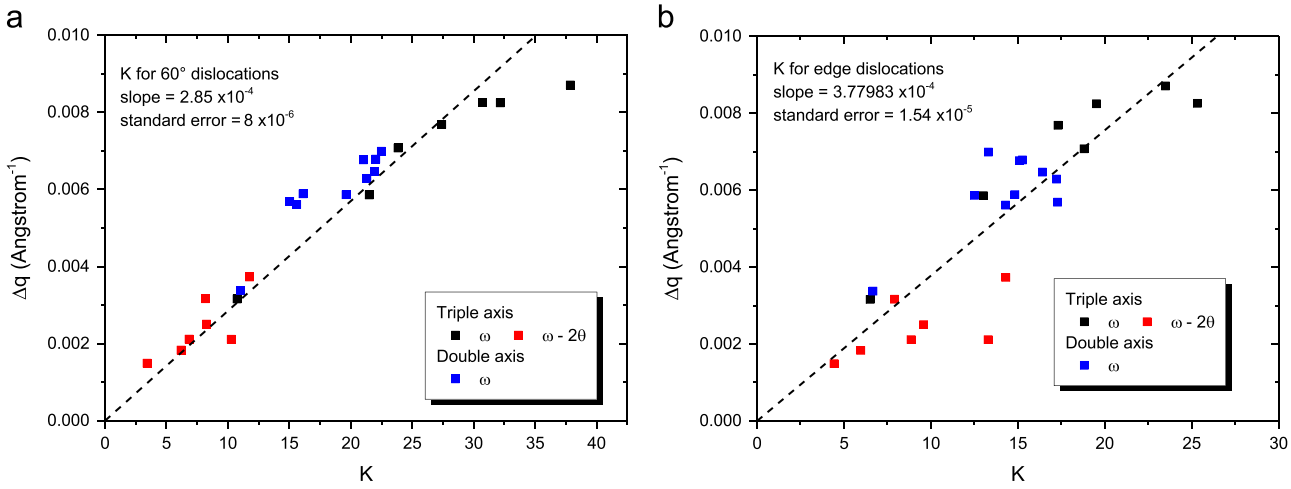

Fig. 6. Modified Williamson-Hall plot using *K* values for 60° dislocations (a) and 90° dislocations (b).

In both cases the data points fall reasonably well on a common straight line, although the alignment appears to be better in the case of *K* values for 60° dislocations. This seems to indicate that the dislocation population in the interfacial network is of mixed type, i.e. both 60° and edge dislocations coexist in the network. Indeed, if only one type of dislocation was involved in the peak broadening, one would obtain a perfect alignment for one type of dislocation and no linear dependence for the other, which is not the case here. This observation mitigates the analysis of the $\overline{2}\,\overline{2}4$ GaSb peak reciprocal space map (leading to the conclusion that edge dislocations are predominant), but is probably the most accurate given the large number of different reflections considered here. The linear fit of the data points in Fig. 6a gives a slope of 2.85×10^{-4}, which is equal to $\sqrt{\frac{\gamma\rho}{d}}$ according to Eq. (1). This result can be understood following the interpretation given in reference [11] reporting results obtained for GaAs on Si hetero-epitaxy. In this paper, the authors consider a regular network of edge dislocations in which randomly positioned 60° dislocations exist and are the main cause for the broadening of the reflection peak. The effect of the periodic array of edge dislocations on the peak broadening can indeed be considered here as negligible: when the ordering of such an array is close to perfection, it produces non-uniform strain in a layer of a few nanometers thick, which are orders of magnitude thinner than the total film thickness. Nevertheless, edge dislocations accommodate twice as much misfit strain than the 60° dislocations, and such a periodic array is therefore the main contributor to the strain relaxation. The same hypothesis (a regular array of edge dislocations coexisting with random 60°) was made in the case described here. A random distribution of dislocations corresponds to a situation where $\gamma=1$, which allows calculating the 60° dislocation density. Based on the slope extracted from Fig. 1a, a linear density of 60° dislocations of $8.1 \times 10^4\ \mathrm{cm}^{-1}$ is calculated for a GaSb layer thickness of 1 μm. On the other hand, in the absence of edge dislocations, the density of 60° dislocations required to completely relax the mismatch between GaSb and Si can be estimated by f/b, where f is the mismatch $((a_{GaSb}-a_{Si})/a_{Si})$ and b is the Burger's vector component along the interface. A layer completely relaxed by 60° dislocations would thus have a linear density of about $4 \times 10^6\ \mathrm{cm}^{-1}$. From the fitting of the data in Fig. 5a, and according to this analysis, we can thus estimate that the 60° dislocations are only responsible for 2% of the total relaxation, which is extremely low, considering that similar experience conducted for the GaAs/Si case (despite a significantly smaller mismatch than for GaSb on Si) has led to values comprised between 9% and 26% depending on the substrate miscut angle [11].

A second interpretation of these results can be made by fitting the data points in Fig. 6b, and was previously used by Reyner et al. [12] for the study of the edge dislocation network at the GaSb on GaAs interface. In this approach, only 90° dislocations are considered, and the perfection of the network is determined by evaluating the γ factor in Eq. (1). In the case of GaSb on Si, the f/b relationship gives a density of $\rho=2.8 \times 10^6\ \mathrm{cm}^{-1}$ to completely relax the strain inside the GaSb layer by a network of edge dislocations having a spacing of 3.5 nm. The slope extracted from data in Fig. 5b (3.78×10^{-4}) can again be compared to $\sqrt{\frac{\gamma\rho}{d}}$, which leads to a spatial correlation factor $\gamma=0.05$. The average variation of the distance between two adjacent dislocations can thus be estimated to be close to 5%, which indicates a relatively well arranged interfacial network of edge dislocations, although the value we found is larger than in the GaSb on GaAs case (~1.5% [12]), which is a system known to have the best ordering of the misfit dislocation array [13]. This higher value is probably due to the larger lattice mismatch or to a different nucleation mechanism. An analysis mixing both kind of dislocation could be done [14], but would be far more complex. In the two approaches developed above, we have considered that the X-ray peak broadening resulted from only one kind of dislocation at a time. In fact, both of them certainly participate to the broadening, and the numbers we found are thus likely to be upper limit values.

3.4. Post-growth annealing

Annealing of highly mismatched hetero-epitaxial structures has been known for a long time to be an efficient way of improving the material quality [15,16]. Reduction of the dislocation density arises due to their annihilation caused by the dislocation movement and coalescence at high temperature.

To study the effect of annealing on the GaSb/AlSb on Si hetero-epitaxial structures, a set of samples with a 5 nm thick AlSb nucleation layer grown at 500 °C and a GaSb layer with thicknesses of 0.1, 0.2, 0.5 and 1 μm also grown at 500 °C was realized. X-ray rocking curves (*double crystal measurement with open detector*) have been measured on as-grown samples, which were then reloaded in the MBE reactor for annealing at 550 °C under Sb flux during 30 min. The process was repeated, and rocking curves measured after 30 min, 1 and 2 h total annealing time. The evolution of the 004 GaSb peak FWHM with the annealing duration is shown in Fig. 7a, for the four GaSb layer thicknesses considered. In each case, one can observe an improvement of the material quality thanks to the annealing. The FWHM first decreases and then starts leveling off, after a duration that visibly depends on the layer

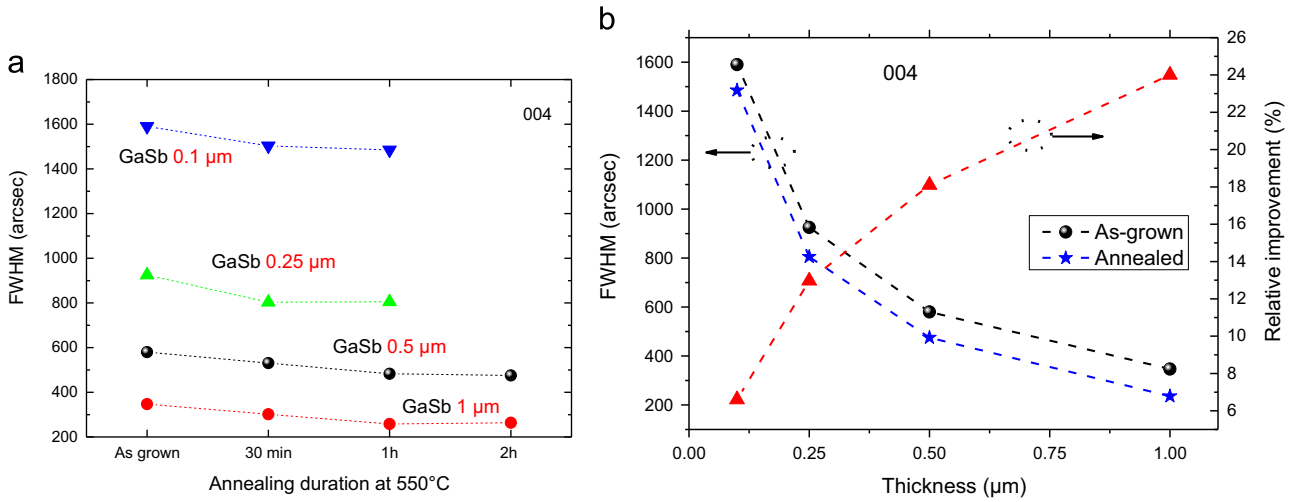

Fig. 7. Variation of the FWHM with the annealing duration for different GaSb layer thicknesses (a); comparison of the FWHM improvement versus the GaSb thickness (b).

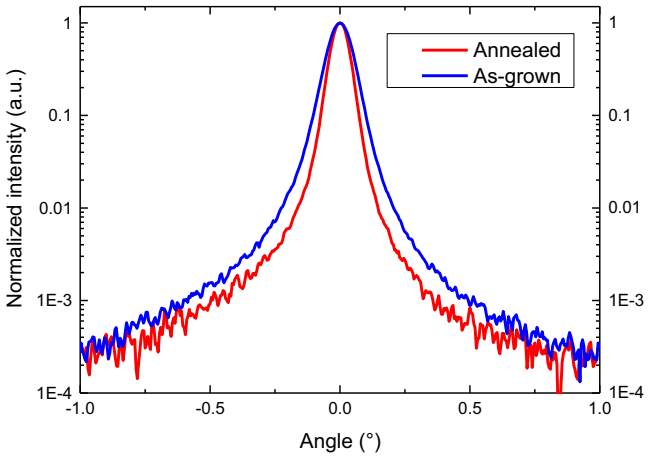

Fig. 8. 004 ω-scans before and after annealing at 550 °C.

thickness. While the annealing of thinner samples can be considered complete after about 30 min, it takes about twice this duration in the case of 0.5 and 1 µm thick samples. A comparison of the results before and after complete annealing is displayed in Fig. 7b. The improvement brought by the annealing increases with the GaSb layer initial thickness, from a reduction of about 7% of the FWHM for the thinnest sample to about 24% for the 1 µm thick layer. Therefore, while an annealing step at the initial stage of the buffer growth seems to only have a marginal effect on the material quality, the improvement becomes quite significant for thicker buffer layers.

Finally, the ω-scans (*double crystal measurement with open detector*) measured on the 1 µm thick sample before and after annealing are compared in Fig. 8. After a complete annealing process, this sample exhibits an excellent FWHM of 235 arcsec, down from the 347 arcsec measured on the as-grown sample. For comparison sake, one can refer to the review paper by Bolkhovityanov et al. presenting the best results obtained in the Ge on Si hetero-epitaxy case (Figure 10 of Ref. [17]). The general trend gives FWHM values for Ge layers of similar thickness (1 µm) grown on Si close to 200 arcsec, and the best result approaches 160 arsec [18]. The direct hetero-epitaxy of GaAs films on Si is also widely documented in the literature. The lattice-mismatch in this case is similar to the growth of Ge on Si, and the best results obtained to date show FWHM of the 004 peaks close to 200 arcsec for a 1 µm thick layer [19]. Despite a much larger lattice mismatch (about 13% compared to about 4%), the FWHM we obtained is thus surprisingly close to state-of-the-art Ge or GaAs on Si. Regarding GaSb on Si, the best result to our knowledge was obtained by Akahane et al. using a similar nucleation layer [6]. A FWHM of 215 arcsec was demonstrated but this value corresponded to a much thicker GaSb layer (2.5 µm instead of 1 µm in our case). Finally, atomic force microscopy carried out on all samples revealed RMS roughness in the 2–10 nm range, without any clear relationship with the XRD FWHM.

4. Conclusion

In conclusion, we have studied by X-ray diffraction GaSb layers grown on silicon substrates by MBE. An AlSb nucleation layer was used to improve the material quality, and several thicknesses and growth temperature were explored to get a better insight on their influence on the GaSb layer quality. We found that a thin (4 MLs) AlSb layer deposited at 450 °C gives the narrowest X-ray diffraction peaks. These results could possibly be further improved by studying the influence of the V/III ratio used during the deposition of the nucleation layer. This parameter certainly impacts the morphology of the AlSb layer and thus the material quality of the subsequently grown layers, and will be explored in future work. We also proposed that the GaSb layer quality depends upon the density of AlSb islands, which improves the GaSb growth by acting as nucleation sites. However, according to our interpretation, the coalescence of the AlSb islands results in the degradation of the GaSb quality, and the best results are thus obtained when the AlSb island density is maximum, just before they start to coalesce. Transmission electron microscopy (TEM) studies will have to be carried out to consolidate this hypothesis. TEM could also provide a better insight on the nature of the interaction between Al and Si during the nucleation (formation of a uniform Al–Si layer, islanding or formation of a eutectic, etc). Analyzing the FWHM of the GaSb diffraction peaks measured on several plane families, we were able to give a preliminary description of the nature of the misfit dislocations. We also studied the use of an Al layer before the GaSb growth and found that it is as efficient as AlSb. Interestingly enough, the results indicate that the quality of the GaSb layer grown using this Al layer is less dependent on the growth temperature, and can be achieved within a reasonable thickness range, making it an attractive alternative to AlSb. The positive effect of post-growth annealing was also demonstrated, and a 1 µm thick GaSb layer with an X-ray peak FWHM of 235 arcsec was obtained using this technique. This FWHM is comparable to the

values obtained with other materials having a smaller lattice-mismatch with silicon (GaAs or Ge for example).

Acknowledgments

This work has been partly supported by ANR under Projects OPTOSi (ANR-12-BS03-002) and ANTIPODE (ANR-14-CE26-0014), and by the French "Investment for the Future" Program (EquipEx EXTRA, ANR-11-EQPX-0016). The help and guidance of V.M. Kaganer regarding the analysis of the data presented in this paper is greatly acknowledged. The authors also acknowledge C. Cornet and A. Letoublon, FOTON-INSA Rennes, and L. Largeau and G. Patriarche, LPN-Marcoussis for useful discussions. E.T. acknowledges support from Institut Universitaire de France (IUF).

References

[1] Nick H. Julian, Phil A. Mages, Chong Zhang, John E. Bowers, Improvements in epitaxial lateral overgrowth of InP by MOVPE, J. Cryst. Growth 402 (2014) 234–242, http://dx.doi.org/10.1016/j.jcrysgro.2014.05.026.

[2] J.R. Reboul, L. Cerutti, J.B. Rodriguez, P. Grech, E. Tournié, Continuous-wave operation above room temperature of GaSb-based laser diodes grown on Si, Appl. Phys. Lett. 99 (2011) 121113.

[3] G. Balakrishnan, S. Huang, L.R. Dawson, Y.-C. Xin, P. Conlin, D.L. Huffaker, Growth mechanisms of highly mismatched AlSb on a Si substrate, Appl. Phys. Lett. 86 (3) (2005) 034105, http://dx.doi.org/10.1063/1.1850611.

[4] Y.H. Kim, J.Y. Lee, Y.G. Noh, M.D. Kim, S.M. Cho, Y.J. Kwon, J.E. Oh, Appl. Phys. Lett. 88 (2006) 241907.

[5] K. Akahane, N. Yamamoto, S. Gozu, A. Ueta, N. Ohtani, Initial growth stage of GaSb on Si(001) substrates with AlSb initiation layers, J. Cryst. Growth 283 (2005) 297–302.

[6] K. Akahane, N. Yamamoto, S. Gozu, N. Ohtani, Heteroepitaxial growth of GaSb on Si (001) substrates, J. Cryst. Growth 264 (2004) 21–25.

[7] S.H. Vajargah, S.G. Tavakoli, J.S. Preston, R.N. Kleiman, G.A. Botton, Growth mechanisms of GaSb heteroepitaxial films on Si with an AlSb buffer layer, J. Appl. Phys. 114 (2013) 113101.

[8] K. Madiomanana, M. Bahri, J.B. Rodriguez, L. Largeau, L. Cerutti, O. Mauguin, A. Castellano, G. Patriarche, E. Tournié, Silicon surface preparation for III–V molecular beam epitaxy, J. Cryst. Growth 413 (2015) 17–24, http://dx.doi.org/10.1016/j.jcrysgro.2014.12.004.

[9] V.M. Kaganer, R. Kohler, M. Scmidbauer, R. Opitz, X-ray diffraction peaks due to misfit dislocations in heteroepitaxial structures, Phys. Rev. B 55 (1997) 1793–1810.

[10] V.M. Kaganer, A. Shalimov, J. Bak-Misiuk, K.H. Ploog, X-ray diffraction peaks from misfit dislocations in double and triple-crystal diffractometry, Phys. Status Solidi A 204 (8) (2007) 2561–2566.

[11] A. Shalimov, J. Bak-Misiuk, V.M. Kaganer, M. Calamiotou, A. Georgakilas, Strain nonuniformity in GaAs heteroepitaxial films on Si(001) studied by x-ray diffraction, J. Appl. Phys. 101 (2007) 013517.

[12] C.J. Reyner, J. Wang, K. Nunna, A. Lin, B. Liang, M.S. Goorsky, D.L. Huffaker, Characterization of GaSb/GaAs interfacial misfit arrays using x-ray diffraction, Appl. Phys. Lett. 99 (2011) 231906.

[13] A.Y. Babkevich, R.A. Cowley, N.J. Mason, S. Weller, A. Stunault, X-ray scattering from dislocation arrays in GaSb, J. Phys.: Condens. Matter 14 (2002) 1305–13528.

[14] A. Benediktovitch, A. Zhylik, T. Ulyanenkova, M. Myronov, A. Ulyanenkov, Characterization of dislocations in germanium layers grown on (011)- and (111)-oriented silicon by coplanar and noncoplanar X-ray diffraction, J. Appl. Cryst. 48 (2015) 655–665.

[15] J.E. Ayers, L.J. Showalter, S.K. Ghandhi, Post-growth thermal annealing of GaAs on Si(001) grown by organometallic vapor phase epitaxy, J. Cryst. Growth 125 (1992) 329–335.

[16] M. Yamaguchi, M. Tachikawa, Y. Itoh, M. Sugo, S. Kondo, Thermal annealing effects of defect reduction in GaAs on Si substrates, J. Appl. Phys. 68 (1990) 4518.

[17] Y.B. Bolkhovityanov, L.V. Sokolov, Ge-on-Si films obtained by epitaxial growing: edge dislocations and their participation in plastic relaxation, Semicond . Sci. Technol. 27 (2012) 043001.

[18] K.W. Shin, H.-W. Kim, J. Kim, C. Yang, S. Lee, E. Yoon, The effect of low temperature buffer layer on the growth of pure Ge on Si(001), Thin Solid Films 518 (22) (2010) 6496–6499.

[19] Y.B. Bolkhovityanov, O.P. Pchelyakov, GaAs epitaxy on Si substrates: modern status of research and engineering, Physics-Uspekhi 51 (5) (2008) 437–456.